

Spatial TCR clonality and clonal expansion in the in situ microenvironment of non-small cell lung cancer

Hui Yu , Anastasia Magoulopoulou, Rose-Marie Amini, Maria Paraskevi Chatzinikolaou, Masafumi Horie, Amanda Lindberg, Artur Mezheyeuski, Max Backman, Andreas Metousis, Hans Brunnström, Millaray Marincevic, Johan Botling, Johanna Sofia Margareta Mattsson, Klas Kärre, Karin Leandersson, Mats Nilsson, Carina Strell, Patrick Micke

To cite: Yu H, Magoulopoulou A, Amini R-M, *et al.* Spatial TCR clonality and clonal expansion in the in situ microenvironment of non-small cell lung cancer. *Journal for ImmunoTherapy of Cancer* 2025;**13**:e012089. doi:10.1136/jitc-2025-012089

► Additional supplemental material is published online only. To view, please visit the journal online (https://doi.org/10.1136/iitc-2025-012089).

CS and PM are joint senior authors.

Accepted 01 August 2025



© Author(s) (or their employer(s)) 2025. Re-use permitted under CC BY-NC. No commercial re-use. See rights and permissions. Published by BMJ Group.

For numbered affiliations see end of article.

Correspondence to

Dr Patrick Micke; patrick.micke@igp.uu.se

Dr Carina Strell; carina.strell@igp.uu.se

ABSTRACT

Background T-cell activation and clonal expansion are essential to effective immunotherapy responses in non-small cell lung cancer (NSCLC). The distribution of T-cell clones may offer insights into immunogenic mechanisms and imply potential prognostic and predictive information.

Methods We analyzed α/β T-cell receptor (TCR) clonality using RNA-sequencing of bulk frozen tumor tissue from 182 patients with NSCLC. The data was integrated with molecular and clinical characteristics, extensive in situ imaging, and spatial sequencing of the tumor immune microenvironment. TCR clonality was also determined in an independent cohort of nine patients with immune checkpoint-treated NSCLC.

Results TCR clonality (Gini index) patterns ranged from high T-cell clone diversity with high evenness (low Gini index) to clonal dominance with low evenness (high Gini index). Generally, TCR clonality in cancer was lower than in matched normal lung parenchyma distant from the tumor (p=0.021). The TCR clonality distribution between adenocarcinoma and squamous cell carcinoma was similar; however, smokers showed a higher Gini index. While in the operated patient with NSCLC cohort, TCR clonality was not prognostic, in an immune checkpoint inhibitor-treated cohort, high TCR clonality was associated with better therapy response (p=0.016) and prolonged survival (p=0.003, median survival 13.8 vs 2.9 months). On the genomic level, a higher Gini index correlated strongly with a lower frequency of epidermal growth factor receptor (EGFR) and adenomatous polypsis coli (APC) gene mutations, but a higher frequency of P53 mutations, and a higher tumor mutation burden. In-depth characterization of the tumor tissue revealed that high TCR clonality was associated with an activated, inflamed tumor phenotype (PRF1, GZMA, GZMB, INFG) with exhaustion signatures (LAG3, TIGIT, IDO1, PD-1, PD-L1). Correspondingly, PD-1+, CD3+, CD8A+, CD163+, and CD138+immune cells infiltrated cancer tissue with high TCR clonality. In situ sequencing recovered single dominant T-cell clones within the patient tumor tissue, which were predominantly of the CD8 subtype and localized closer to tumor cells.

WHAT IS ALREADY KNOWN ON THIS TOPIC

Specific T-cell activation and clonal expansion are critical components of an effective anticancer immune response. This active response is reflected by the frequency and distribution of T-cell clones within the local tumor microenvironment.

WHAT THIS STUDY ADDS

⇒ Our study demonstrates that T-cell clonal expansion, as quantified by the Gini index, is variably present in non-small cell lung cancer tissue and is associated with an active immune phenotype and the spatial proximity of CD8+T cells to cancer cells. High T-cell receptor clonality was predictive for improved response and survival following immune checkpoint blockade.

HOW THIS STUDY MIGHT AFFECT RESEARCH, PRACTICE OR POLICY

⇒ The measurement of T-cell expansion provides clinically relevant information for lung cancer patients. The development of T-cell clonality testing on minimal diagnostic formalin-fixed, paraffin-embedded biopsies holds the potential to refine patient stratification for immunotherapy and may also aid in identifying tumor-specific antigens for personalized immune interventions.

Conclusion Our robust analysis pipeline characterized diverse TCR repertoires linked to distinct genotypes and immunologic tumor phenotypes. The spatial clustering of expanded T-cell clones and their association with immunological activation underscores a functional, clinically relevant immune response, particularly in patients with NSCLC treated with checkpoint inhibitors.

INTRODUCTION

The introduction of new immune modulatory treatment options has revolutionized clinical oncology and provided clinical



evidence that the immune system is able to recognize and eliminate cancer cells. ¹ In line with this, the infiltration of immune cells in tumor tissue is associated with an improved prognosis, independent of therapy.^{3 4} This includes densities of T-cell subsets (CD4, CD8, T regulatory (Treg) cells, CD45 T memory cells), B cells, plasma cells, as well as subsets of macrophages and dendritic cells.^{5–7} This particular immune cell infiltration is often associated with higher expression of T-cell activation markers but also of T-cell exhaustion.^{8–10} This immune cell-dense tumor tissue is frequently denoted as "immune hot" or "inflamed" and is not only prognostic but has also proven to be predictive in the context of immune checkpoint blockade. 6 11-14 However, the prognostic and predictive value is still relatively low, which suggests that these quantitative measurements do not entirely reflect the patient's individual actual immune reaction. Furthermore, technical aspects and the heterogeneity of results hinder clinical implementation.

The efficacy of a specific tumor-antigen T-cell response is reflected by the precedent activation, differentiation, and clonal expansion of naive T cells on specific binding of their T-cell receptors (TCRs) to tumor-antigens presented on major histocompatibility complex (MHC), together with costimulatory signals (eg, CD28). The activation is reinforced by autocrine or paracrine interleukin (IL)-2 signaling, contributing to massive clonal expansion of tumor-antigen specific T-cell clones generating both effector and memory T cells. This T-cell activation, with subsequent expansion, can be measured by the clonal unevenness of the TCR in the T-cell population, which is often referred to as high clonality.

TCR clonality was previously determined by targeted sequencing of the TCR-ß chain. Clinically certified assays are used to determine malignant clones in hematological malignancies that can be followed over time. In solid tumors, targeted sequencing methods have mostly been done on blood samples to evaluate specific antitumor T-cell responses and their relation to clinical outcomes. In melanoma, tumor TCR clonality was associated with benefit from checkpoint inhibitor treatment in several studies.

Recently, bioinformatic algorithms have been developed to determine the clonality in crude RNA sequencing (RNA-seq) data without the necessity of specific assays. 30 31 Such RNA-seq-based clonality analysis of lung cancer tissue indicated that the TCR richness, that is, the number of different T-cell clones, was lower in the tumor tissue than in the adjacent normal tissue and was associated with histomorphological tumor features. 32 However, T-cell repertoire analysis was most often limited to the in silico processing of public data sets, and consequently, the pure quantification of the T-cell clones excluded the cellular tissue context. It can be speculated that the TCR clonality and differentiation also depend on molecular features of tumor and stroma cells and that the individual immune microenvironment is a cause or consequence of a specific T-cell expansion. This was recently demonstrated

Table 1 Patient characteristics of the non-small cell lung cancer cohort. Patients were operated on at the Uppsala University Hospital (Sweden) between 2006 and 2010. Fresh tissue was procured freshly after the operation and used later for RNA sequencing.

later for RNA sequencing.		
	No.	%
All patients	182	100
Age (years)		
>70	73	40
≤70	109	60
Sex		
Female	95	52
Male	87	48
Smoking		
Ever smokers	165	91
Never smokers	17	9
Histology		
Adenocarcinoma	107	59
Squamous cell carcinoma	62	34
Other types	13	7
Stage (eighth edition)		
1A2	39	21
1A3	35	19
1B	23	13
2A	14	8
2B	30	17
3A	35	19
3B	6	3
Performance status (WHO)		
0	114	63
1	66	36
2	2	1

in an elegant study characterizing "supportive" and "non-supportive" CD8 T-cell niches in different cancer types. 33

With this background, our study aimed to determine the T-cell repertoires in the immune microenvironmental context using a thoroughly validated TCR sequencing pipeline,³⁴ providing the clinical and molecular background of T-cell clonality in cancer tissue from patients with non-small cell lung cancer (NSCLC).

MATERIALS AND METHODS Patient material

This study includes 182 patients with NSCLC from the Uppsala II cohort (n=357) for which RNA-seq data were available, as described before. ³⁵ Patient characteristics are listed in table 1 and online supplemental table S1. All patients from the Uppsala II cohort were patients with NSCLC treated surgically at Uppsala University Hospital between 2006 and 2010. This study was conducted in

accordance with the Declaration of Helsinki and the Swedish Ethical Review Act.

RNA-seq data from publicly available NSCLC cohort downloaded from Gene Expression Omnibus (GSE126044) were also used. These RNA-seq data are derived from nine fresh frozen samples from patients with anti-programmed cell death protein-1 (PD-1) (nivolumab) treated NSCLC (online supplemental Table $S3).^{36}$

RNA sequencing

Transcriptomic profiling was performed on fresh frozen tumor tissue, as described previously.35 RNA was extracted using RNeasy Mini Kit (Qiagen) from archived fresh frozen tumor tissues stored at -80°C. The samples were prepared for sequencing using the Illumina TruSeq RNA Sample Prep Kit V.2 and poly-A selection. 100 base paired-end multiplex sequencing was performed on the Illumina HiSeq2500 machine (Illumina, USA) with five samples per lane following the standard Illumina RNA-seq protocol. The raw data is accessible in the Gene Expression Omnibus (GEO) repository (accession number GSE81089).

TCR clonality analysis

TCR clones within each sample were extracted from bulk RNA-seq results using MiXCR V.3.0.13 following the software reference document (https://docs.milaboratories.com/) on a Windows V.10 system server (Java V.17.0.2, processor: Intel i9-11900). Raw RNAseq data was aligned with the command "mixcr align -s hs -p rna-seq -OallowPartialAlignments=true forward_ sequence reverse_sequence align_output.vdjca". After that, two rounds of "assemblePartial" were performed according to the software reference document with "mixcr assemblePartial align_output. commands vdjca assemble1.vdjca" and "mixcr assemblePartial assemble1.vdjca assemble2.vdjca". The extension step was then performed using the command "mixer extend assemble2.vdjca extend.vdjca". Clones were assembled using "mixcr assemble extend.vdjca clones. clns". TRA and TRB clones were exported separately using the commands "mixcr exportClones -cloneId -count -fraction -vGene -dGene -jGene -cGene -vAlignment -jAlignment -targets -nFeature CDR3 -c TRA clones.clns tra.txt" and "mixcr exportClones -cloneId -count -fraction -vGene -dGene -jGene -cGene -vAlignment -jAlignment -targets -nFeature CDR3 -c TRB clones.clns trb.txt". TRA and TRB clones for each sample were merged, and a fraction of each clone was recalculated using a Python script. Clonality was quantified using the Gini coefficient (Gini index)²⁰ 21 and calculated based on the sequences of both beta and alpha chain using a Python script.

$$\label{eq:Gini Index} \text{Gini Index} = \; \frac{\sum_{i=1}^{n} \sum_{j=1}^{n} \left| x_i - x_j \right|}{2n^2 \overline{x}} \; \left(x_i \; \text{represent the clone count for clone } i \right)$$

All scripts are available as Online supplemental material and have been deposited on GitHub. The workflow of this analysis is provided in online supplemental figure S1. The quality control of the MiXCR analyses for each case from the Uppsala cohort and the external cohort is provided in the online supplemental file 1. The Gini index, the number of unique alpha/beta T-cell clones detected, and clinical data for each patient are included in online supplemental table S1. The detected TCR sequences for all TCR clones for each case can be downloaded at https://doi.org/10.5281/zenodo.15439669.

Differential gene expression analysis

The differential gene expression analysis was performed using the "DESeq2" package (V.1.40.2) in R. Two groups were compared: the top quartile against the bottom quartile of patients ranked by Gini index. The gene expression raw count data and the patient group records were formed as required by the software instruction. "DESeqDataSetFromMatrix", "DESeq", and "results" from the "DESeq2" package were used with the default function. The full result is shown in the online supplemental Table S3. The Gene Ontology (GO) and Kyoto Encyclopedia of Genes and Genomes (KEGG) analysis was performed using "enrichGO" and "enrichKEGG" with default parameters from package "clusterProfiler" (V.4.8.2).

Lymphotrack

Four patients with different clonality/Gini index were analyzed by the Lymphotrack assay.²³ Two cases with the highest Gini index were selected to represent the high T-cell clone expansion cases. One case with the median Gini index of all cases was selected to represent the median T-cell clone expansion cases. One case with the lowest Gini index was selected to represent the low T-cell clone expansion cases. Three 10 µm fresh frozen tissue sections of each patient sample were transferred into ATL buffer, and DNA was extracted using DNeasy Blood and Tissue kit (Qiagen Germany) following the manufacturer's protocol. Extracted DNA was stored in 100 µL AE buffer, and the concentration was measured by the Qubit V.2.0 Fluorometer (Invitrogen) using Qubit dsDNA BR Assay Kit (Invitrogen, USA) according to the manufacturer's protocol. TRB and TRG clones were measured respectively using LymphoTrack Dx TRB Assay Kit A-MiSeq (Invivoscribe, USA) and LymphoTrack Dx TRG Assay Kit Panel-MiSeq (Invivoscribe) on the Illumina MiSeq sequencing platform. Raw sequence data was analyzed and visualized using the LymphoTrack Software-MiSeq (V.2.4.3, Invivoscribe).

Immunohistochemistry

Immunohistochemistry was used to quantify immune cell infiltration and immune marker expression in this lung cancer cohort, as described previously. 12 35 37 The detailed staining protocol is available on the Human Protein Atlas website (www.proteinatlas.org/download/IHC_protocol. pdf). Formalin-fixed, paraffin-embedded (FFPE) tissue microarrays (TMA), including two 1 mm (diameter) representative punches of each patient, were cut to 4µm sections. Automated immunohistochemistry (IHC) was conducted using the Autostainer 480 (Thermo Fisher Scientific, USA) as described before, 12 35 the antibodies used were: CD3 (CL1497, 1:1000 dilution, Atlas Antibodies), CD4 (CL0395, 1:125 dilution, Atlas Antibodies), CD8A (CL1529, 1:250, Atlas Antibodies), CD20 (L26, preprepared manufacturer dilution; Agilent Technologies, USA), CD45RO (UCHL1, 1:1000 dilution; Abcam, UK), CD138 (MI15, 1:100 dilution; Agilent Technologies), CD163 (10D6, 1:100 dilution; Novocastra, Leica Biosystems, USA), FOXP3 (236A/E7, 1:15 dilution; Santa Cruz Biotechnology, USA), PD-1 (MRQ-22, 1:100 dilution; Cell Marque, USA), and NKp46 (195314, 1:50 dilution; R&D Systems, USA). PD-L1 (22C3, ready-to-use solution, Agilent Technologies) staining was performed at the Clinical Pathology Unit at Uppsala University Hospital on a DAKO autostainer system according to manufacturer instructions.

Afterward, vision-based manual annotation was carried out to calculate the immune score on the stroma and tumor area of each TMA core, as described before. 12 37 38 The immune score was calculated by dividing stained, positive immune cells by all other cells in the stroma or tumor compartment, respectively. The programmed death-ligand 1 (PD-L1) staining annotation in the tumor compartment followed the standard annotation of cancer cell staining used in clinical diagnostics, in which partial or complete membrane-stained tumor cells were all counted positive.

Multiplex immunofluorescence

Multiplex immunofluorescence (multiplex IF) staining was used to quantify and localize immune cell subsets in this patient with NSCLC cohort as previously described. 638 In brief, TMA sections were stained with antibody panels: a tumor-infiltrating lymphocyte panel, including CD4, CD8, CD20, FoxP3 and PanCK; a natural killer (NK) cell/ macrophage panel, including CD3, NKp46, CD56, CD68, CD163 and PanCK; and an antibody presenting cell panel (APC), including CD1a, CD208, CD123, CD15, CD68 and PanCK. The staining procedure was performed in accordance with an earlier published study^{37 38} based on the modified Opal Multiplex IHC assay (Akoya Biosciences, USA). The slides were scanned using the VectraPolaris system (Akoya Biosciences) at a two pixels/µm resolution in multispectral mode and analyzed in the inForm software, where spectral unmixing was used to generate an oligo-layer image with layers corresponding to the specific staining, 4',6-diamidino-2-phenylindole (DAPI), and autofluorescence. The inForm software was used to define tumor and stroma compartments within each tissue core. The algorithm was trained on pathologistannotated samples. Cell segmentation was based on DAPI nuclear staining. Representative subsets of the included markers were annotated as either positive or negative, and the inForm software was then trained on these to

phenotype all other cells accordingly. The intensity of each marker expression was used to calculate the thresholds for marker positivity. A pathologist reviewed each image and curated it with regard to artifacts, staining defects and necrosis.

Mutation analysis

As described previously,³⁹ genomic DNA was extracted from fresh frozen tissue, using the QIAamp DNA Mini Kit (Qiagen) or the QIAamp DNA FFPE Tissue (Qiagen), respectively. Targeted DNA enrichment was performed using the HaloPlex target enrichment system (Agilent Technologies), and targeted deep sequencing was conducted on the Illumina HiSeq 2500 platform following the manufacturer protocol. La Fleur *et al* performed downstream analysis and identified gene variants as published before.

In situ sequencing

The sequencing was performed with modification as previously described. Tumor sections (10 µm) from frozen tumor tissue slides were thawed and air-dried at room temperature for a maximum of 5 min. Fixation was performed with 3.7% formaldehyde for 10 min and the samples were rinsed two times in phosphate-buffered saline (PBS). Permeabilization followed immediately, using 0.1 M hydrochloric acid diluted in water, at room temperature for 5 min. Two PBS washes followed, each lasting 1 min, and then dehydration with 70% and 100% ethanol for 2 min each. After air drying, SecureSeal Hybridization chambers by Grace Bio-Labs were mounted on the tissue sections.

The padlock probe hybridization and rolling circle amplification (RCA) were performed according to the High Sensitivity Library Preparation Kit by Cartana (Cartana, 10x Genomics, USA). In brief, the padlock probe mix (including the Immune General P/N: 4121–13 Lot: 4WW44632, Immune Oncology P/N:4122–13 Lot:4QZ44362, and TCR padlock probe panels together with blocking probes for the high expressors IGKC, PTPRC, and LST1, (online supplemental Tables S10 and S11) was diluted in Buffer A, and incubated at 37°C overnight. On the second day of the protocol, a 30 min wash with WB4 at room temperature and a 2-hour ligation with RM2 and enzymes 1 and 2 at 37°C was performed. The RCA step was then carried out overnight at 30°C with RM3 and enzyme 3 mix.

The procedure continued with the hybridization of L-probes and detection probes on the RCPs, using Cartana's In Situ Sequencing Kit (Cartana). Initially, the samples were incubated with the L-probe mix for an hour at 37°C and washed three times with PBS. Next, they were incubated with the detection oligo mix for an hour at 37°C and again washed three times with PBS.

Autofluorescence was reduced with Vector True-View from Vector Laboratories (Vector Laboratories, USA), as per the manufacturer's protocol. Cover slips were mounted with SlowFade Gold antifade reagent by



Invitrogen (Invitrogen Corp, USA). Lastly, the protocol included cover slip removal and detection oligo stripping between imaging rounds, with 100% formamide for three 1 min incubations, as outlined by Cartana's In Situ Sequencing Kit.

Image acquisition and data processing were performed as described previously.⁴⁰ The entire code is available at https://github.com/Moldia/Lee_2023. The probes were listed in online supplemental tables S10 and S11.

Hexbin-based in situ sequencing data analysis

The analysis of the sequencing result was performed with Python code (V.3.10.13, https://github.com/JnuYHui/ TCR_in_NSCLC). The DAPI image from sequencing was segmented by hexagon bins (long diagonal 300 µm). The sequencing signals were allocated to each hexbin according to their coordinates. The H&E staining was performed on the same slide after imaging for DAPI staining according to the standard H&E staining protocol. The H&E staining slides were scanned using bright field scanning and overlayed to the DAPI image using QuPath (0.5.1) and Python scripts. The hexbins with either EPCAM or CDH1 expression (cut-off=2 signal counts) were assigned as tumor compartment. The empty or necrotic areas were manually annotated. The remaining hexbins were assigned as stroma compartments. TCR clones were considered dominant with a count larger than 10 in the bulk RNA-seq data. TCR clones were recovered in the in situ sequencing data using Python scripts, and the number of dominant clones was counted in each tumor and stroma hexbin and differences were assessed by χ^2 test. Dot plots were made using Python scripts and illustrate the fraction and expression distribution of TCR clones. The stack plots were made in OriginPro2024b (OriginLab Corporation, Massachusetts, USA).

Statistics and bioinformatics

Data analysis was performed using R (V.4.2.0). Median TCR clonality (Gini index=0.25431) was used as a cut-off to define high and low clonality. Statistical significance was set to p<0.05. An unpaired Wilcoxon rank-sum test was used to compare two independent groups, while the unpaired Kruskal-Wallis test was used for more than two independent groups. Boxing plots and the significant test were produced with the ggplot2 package (V.3.3.6). Overall survival analysis was performed using the Kaplan-Meier method with R package "survival" (V.3.3-1) and "survminer" (V.0.4.9) using the log-rank test for group comparison. Multivariate Cox regression test from the "survival" package was used to calculate the relative HRs with 95% CI controlling for all causes. The best cut-off calculation was performed using the "surv_cutpoint" function from the "survminer" package. Spearman's rank correlation between Gini index and the immune markers was calculated using the Hmisc package (V.4.7–1). Hierarchical cluster analysis was carried out using "ward.D2" as a clustering method measuring the Euclidean distance using the "pheatmap" package (V.1.0.12). The DESeq2

package (V.1.36.0) was used to perform differential gene expression. GO and KEGG analysis of the significantly differentially expressed genes was performed using the clusterProfiler package (V.4.4.4). X² tests were used comparing the fraction of dominant TCR clones in tumor and stroma hexabins (Python). The Python and R scripts were deposited at GitHub (V.3.10.13, https://github.com/JnuYHui/TCR_in_NSCLC).

RESULTS

The T-cell repertoire in lung cancer

The T-cell repertoire was determined on RNA-seq data derived from 182 tumor tissues from operated patients with NSCLC (table 1). Additionally, 20 paired normal lung tissues distant from the primary tumor were analyzed. Quantifying RNA reads attributed to each TCR determines the relative frequency and proportion of TCR clones in each sample. These proportions are then visualized using pie charts (figure 1A).

To transfer the pattern of T-cell clones to a metric, we applied the Gini coefficient (Gini index).²⁰ The Gini index is considered particularly useful for describing unevenness.⁴² A T-cell repertoire with few dominant clones results in a high Gini index, whereas a repertoire without dominant clones, with even distribution, results in a low Gini index (figure 1A, online supplemental table S1). In our dataset, the Gini coefficient also provides a larger variance compared with entropy, indicating a higher sensitivity to detect unevenness (online supplemental figure S1).

Using the DNA-based LymphoTrack assay,²³ we recovered the identified dominant clones in four selected samples (online supplemental figure S2). The agreement demonstrates the validity and robustness of our method, as well as the quality of the RNA data sets. The workflow for the calculation of the Gini index (online supplemental figure S1), as well as the CDR3 characteristics of four cases, is provided (online supplemental figure S3).

The RNA-seq analyses of the 182 NSCLC cases revealed a heterogeneous distribution among samples, with a few exceptions, with a median Gini index of 0.25. The distribution of T-cell clonality was similar between adenocarcinoma and squamous cell cancer (figure 1B). The clonality of 20 corresponding normal lung tissue from the same patient revealed generally higher Gini coefficients than tumors (p=0.021, figure 1C).

TCR clonality and association with clinical parameters

Subsequently, we analyzed whether TCR clonality was associated with clinical characteristics. None of the evaluated parameters (patient age, stage, and sex) correlated with the Gini index (online supplemental figure S3 and S4), with the exception that eversmokers revealed a higher TCR receptor clonality in

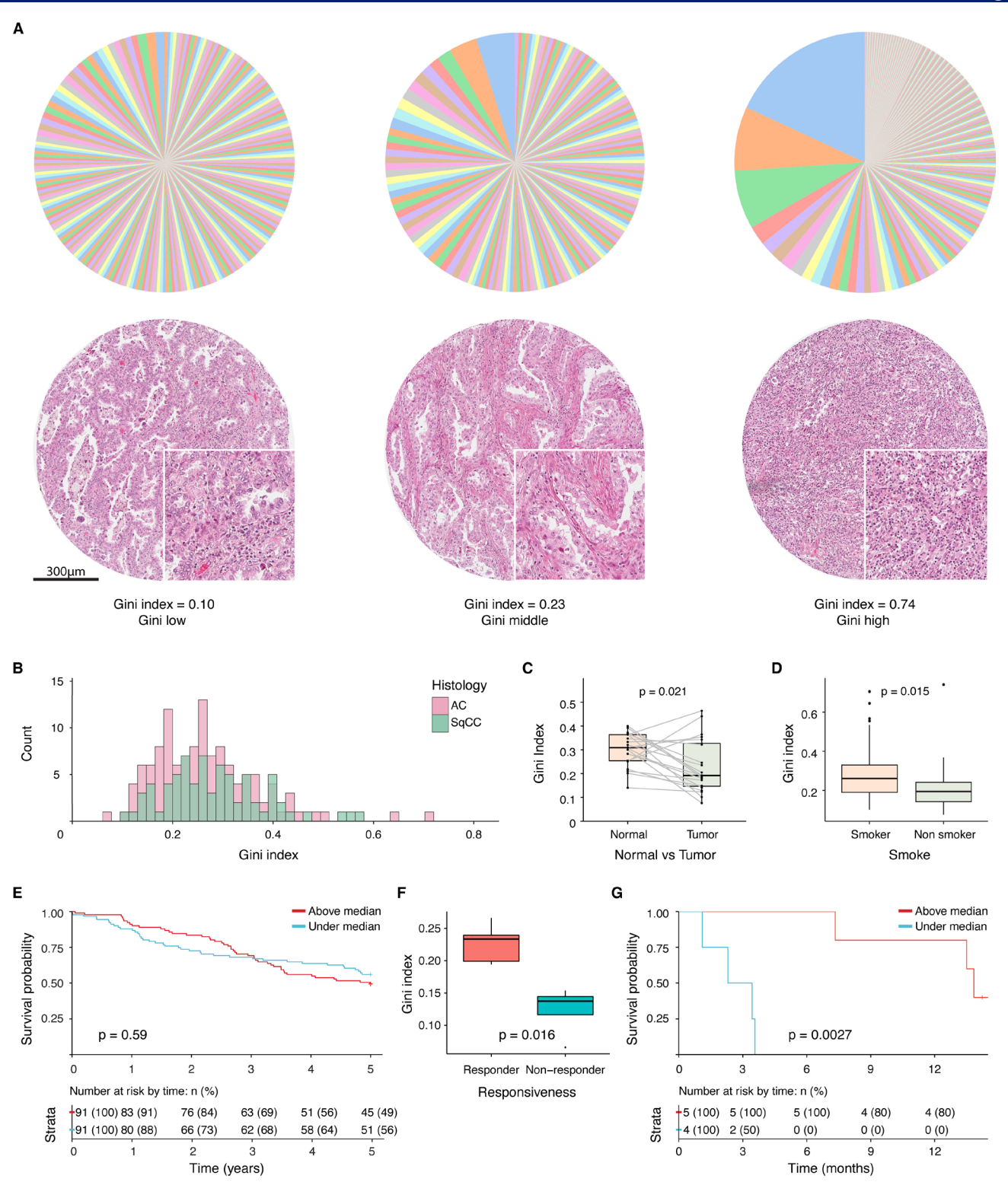


Figure 1 TCR clonality in tumors of patients with NSCLC. (A) Example of different TCR profiles from low Gini index to high Gini index. The pie chart indicates the fraction of each clone within the repertoire of each sample. The corresponding H&E staining of corresponding formalin-fixed, paraffin-embedded tissue. (B) The Gini index distribution histogram of two major types of NSCLC, lung adenocarcinoma (AC) and squamous cell carcinoma (SqCC). (C) Boxplot represents the paired comparison of Gini index between tumor and adjacent normal lung tissue (paired Wilcoxon signed-rank test, n=20). (D) Boxplot presents the difference in the Gini index between never-smokers and smokers. (E) Kaplan-Meier survival analysis of operated patients with NSCLC stratified based on the Gini index using median cut-off (cut-off=0.25). (F) Analysis of patients with advanced NSCLC who received immune checkpoint inhibitor treatment (GSE126044, n=9). Box plot for comparison of responders (n=5; partial response and complete response) and non-responders (n=4; stable disease and progressive disease). (G) Kaplan-Meier survival analysis of same patients with immune checkpoint inhibitor treated NSCLC stratified by median Gini index cut-off (cut-off=0.19). NSCLC, non-small cell lung cancer; TCR, T-cell receptor.

their tumors compared with never-smokers (p=0.015, figure 1D).

T-cell clonality and impact on survival response for immune checkpoint inhibitors

In 182 patients with NSCLC who underwent surgery, the Gini index did not show a significant prognostic impact (p=0.59, median cut-off, figure 1E). This was also true when the Gini index was analyzed as a continuous variable in the univariable Cox regression (HR: 0.89, 95% CI: 0.58 to 1.36, p=0.59) and multivariable Cox regression model (adjusted to age, stage, and performance status, HR: 0.95 (95% CI: 0.62 to 1.47), p=0.83, (online supplemental table S2).

To test the hypothesis that checkpoint inhibitor therapy is particularly effective in patients with higher TCR clonality, that is, tumors with high T-cell expansion, we evaluated an immune checkpoint inhibitor (ICI) treated cohort of patients with NSCLC (n=9; online supplemental table S3) with publicly available RNA-seq data.³⁶ The Gini index was significantly higher in patients who responded to checkpoint inhibitor treatment (figure 1F). This association was also seen in the survival analysis of these patients with advanced NSCLC, with a difference in median survival of 13.8 compared with 2.9 months (log-rank test; p=0.0027, figure 1G). The data thus indicate that TCR clonality does not have a prognostic but a predictive impact in the context of immunotherapy.

The T-cell repertoire in the molecular background of lung cancer

The mutation data of 82 lung cancer-related genes were previously determined by targeted sequencing³⁹ (online supplemental table S4; figure 2A). We found that the Gini index was higher in tumors harboring p53 (p=0.001, false discovery rate (FDR) =0.023), ARID1A (p=0.009, FDR=0.18), EPHB6 (p=0.024, FDR=0.38), and CSMD3 mutations (p=0.031, FDR=0.41). The Gini index was lower for patients with EGFR (p<0.01, FDR=0.024) and APC mutations (p<0.01, FDR=0.03). Notably, the Gini index showed a significant positive correlation with the estimated tumor mutation burden (figure 2B, r=0.27, p<0.001). Taken together, the genetic background of the tumor and the number of putative neoantigens have a relation to the TCR clonality in the local tumor environment and might indicate some tumor-specific reactions.

The T-cell repertoire and the immune landscape of lung cancer

Subsequently, we evaluated the association between the Gini index and the immune cell repertoire in the microenvironment. This was previously done using immunohistochemistry on a tissue microarray with representative tissue cores from the same tumors. 12 Unsupervised hierarchical cluster analysis using the immune scores demonstrated two distinct clusters for patients with high immune scores (n=52) and lower immune scores (n=124) for CD4, CD8, CD20, CD45, CD163, FOXP3, PD-1, and PD-L1 (Wilcoxon test, p<0.01) (figure 3A; online supplemental tables S5 and S6). A higher Gini index was strongly associated in the immune-hot (inflamed) cases (figure 3B, p<0.001). When tumor-infiltrating immune cells were analyzed separately, association to high TCR clonality was more pronounced in the tumor compartment compared with stromal compartment (figure 3C). High Gini index was strongly associated with CD3 positive lymphocytes (p<0.001), PD-1 (p<0.001), CD8 (p<0.001), CD45RO (p<0.001), and CD163 positive cells (p<0.001) in the tumor compartment. Likewise, PD-L1 expression (p<0.001) and PD-1 expression (p<0.01; figure 3C) were associated with higher TCR clonality.

By using an established multiplex immune fluorescence pipeline, we were also able to subtype relevant immune cell populations, indicating that predominantly effector CD8 and CD4 cells, and Treg cells strongly associated with the Gini index (p<0.001, figure 3D), although the association of TCR clonality with Treg cells was restricted to the stroma compartment. In line with the cell density analysis, the distance analysis confirmed that the T-cell clonality is higher when effector CD8 cells are closer and CD4 T regulatory cells in distance to the tumor cells (p<0.001, figure 3E). Of non-lymphocytic cell types, particularly, the number of pro-inflammatory M1-like macrophages correlated with higher T-cell clonality (p<0.01, figure 3D) possibly linking M1 macrophages to antigen presentation.

The Gini index is not only related to the absolute numbers of immune cell types, but also correlates with a higher relative proportion of effector CD8 cells in the

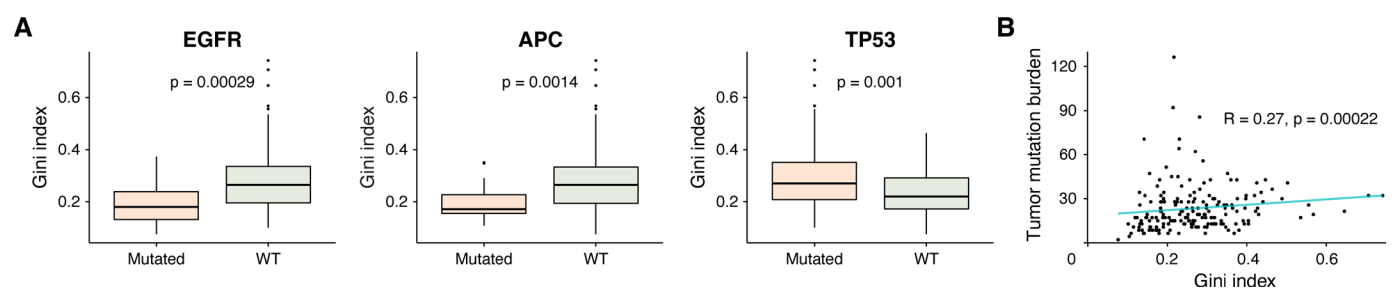


Figure 2 T-cell receptor clonality and association with mutations. (A) Comparison of Gini index between patients with tumors harboring pathogenic mutations (EGFR, APC, TP53) and tumors without mutations (wildtype, WT). (B) Correlation plot between Gini index and estimated tumor mutation burden. APC, adenomatous polypsis coli gene.

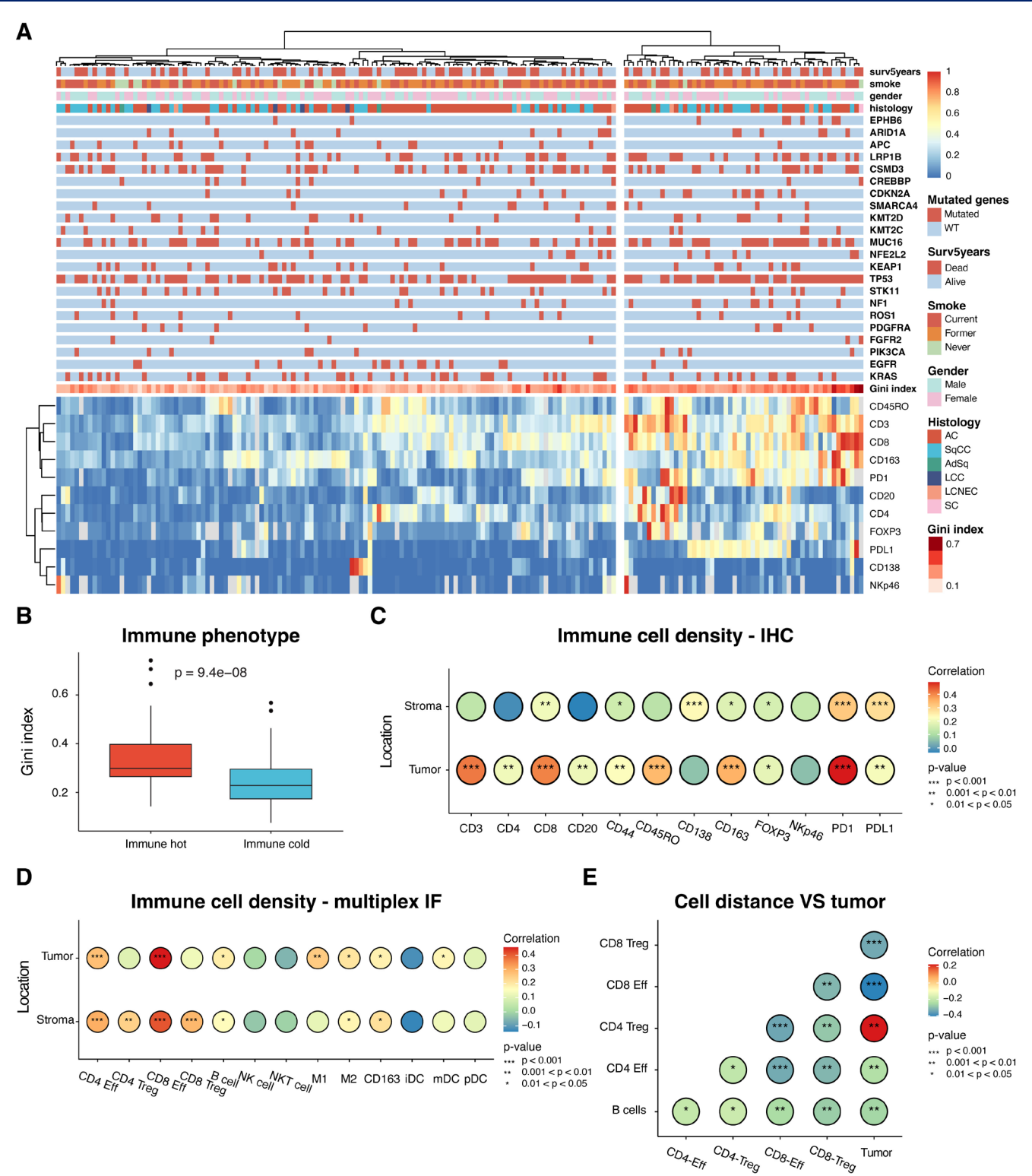


Figure 3 Association of TCR clonality with immunophenotypes. (A) Unsupervised hierarchical cluster analysis based on normalized immune markers expression scores assessed using the immunohistochemical tissue staining of the Uppsala cohort. Patients were stratified into immune hot and immune cold phenotypes. The 5-year survival (Surv5years), clinical parameters, mutation status for selected genes, and their Gini index were given. (B) The Gini index of immune hot and cold tumors was compared. (C) Immune scores based on immunohistochemical stainings of immune markers were associated with the Gini index for the tumor and stroma compartment separately. The correlation level is indicated by the color. (D) Immune cell densities based on multiplex IF were correlated with the Gini index for the tumor and stroma compartment. (E) The cell nearest neighbor distances between each immune cell type and tumor cells were correlated with the Gini index. Red color indicates a longer distance between CD4 Treg cells and tumor cells in cases with higher Gini index. IHC: immunohistochemistry, IF: immunofluorescence, CD4-Eff: CD4 effector cells, CD4-Treg: CD4 regulatory cells, CD8-Eff: CD8 effector cells, CD8-Treg: CD8 regulatory cells.

immune environment (online supplemental figure S3C), indicating a general change of the immune status.

The observation that the local TCR repertoire and immune phenotypes are interconnected was confirmed in gene enrichment analysis based on RNA-seq data from the top quartile cases with the highest Gini index and

the bottom quartile with the lowest Gini index. Higher Gini index demonstrated enrichment of genes related to T-cell activation and expansion, with antigen presentation and binding as well as cytokine signaling. Also, NK cell-mediated immunity (*KLRC1*, *KLRC2*, *KLRC3*, *KLRC4*, *NKG7*) was over-represented in this analysis (figure 4A)

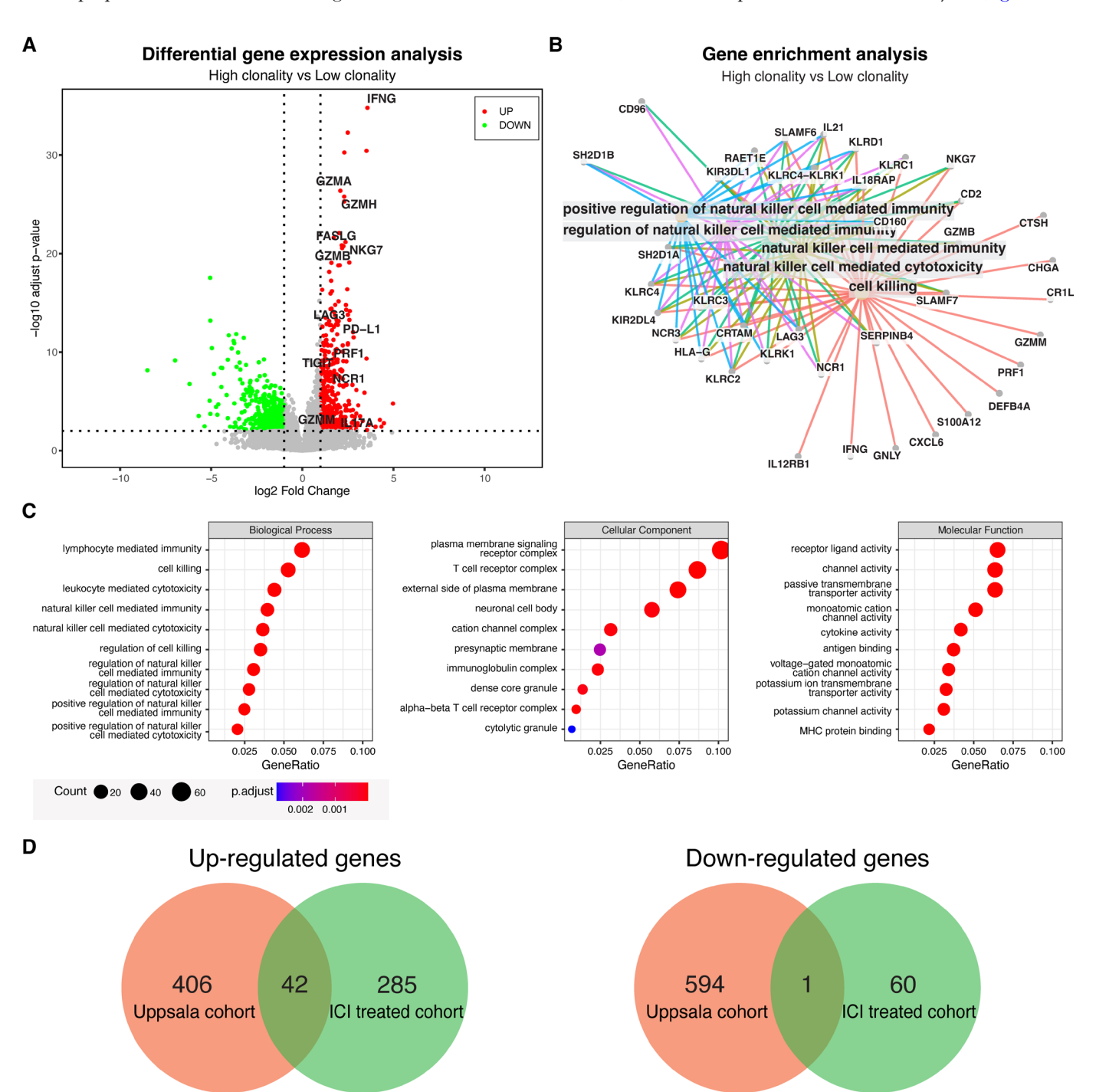


Figure 4 Differential gene expression and gene enrichment analysis. (A) Volcano plot indicating the differently expressed genes (adjusted p value<0.01) in the top 25% high Gini index tumors compared with 25% cases with the lowest Gini index. The upregulated genes were visualized in red and downregulated in green. Selected genes were labeled. (B) Enrichment plot for connection between differentially expressed genes and their pathway. (C) Enrichment plots indicate the biological pathway, cellular component, and molecular function in which differentially expressed genes were involved. Gene ratio (GeneRatio) indicates the percentage of genes involved in the differentially expressed gene set. (D) Venn diagram of genes that are upregulated or downregulated in the operated patients from the Uppsala cohort and immune checkpoint inhibitor treated cohort. MHC, major histocompatibility complex.

and B; online supplemental table S7). In general, genes that were typically associated with immune activation (*PRF1*, *GZMB*, *GZMA*, *INFG*, *IL17*, *NCR1*) were contrasted by inhibitory signals (*LAG3*, *PD-1*, *TIGIT*, *IDO1*) as an indication for T-cell exhaustion (figure 4C).

These findings were confirmed in the independent cohort of ICI-treated patients. With the same pipeline as the Uppsala cohort, differential gene expression analysis of this messenger RNA (mRNA) data set confirmed that TCR clonality was associated with markers of T-cell activation (*GZMA*, *PRF1*, *IL2RB*) and exhaustion (*CD244*, *CD96*); and also involved NK cell immunity (*KRLB1*, *KLRK1*, *KKG7*) (figure 4D, online supplemental tables S8 and S9).

Collectively, we demonstrated that TCR clonality is strongly related to immune activation, a higher immune cell infiltration with effector cells in the tumor cell compartment, eventually counter-regulated by inhibitory signaling and immune cells with signs of T-cell exhaustion.

Location of dominant T-cell clones in the in situ environment of cancer

Recent advances in in situ sequencing techniques allow us to precisely localize gene expression in the cancer microenvironment. Here, we use this technique to recover the gene sequence of the CDR3 TCR region of dominant clones in patients' cancer tissue (figure 5A). We identified the location of the expanded, dominant T-cell clones as well as minor non-dominant clones. By overlaying corresponding H&E stainings, we annotated tumor and stroma cells compartments based on EPCAM and CDH1 mRNA expression (figure 5B, online supplemental tables S10 and S11). Using spatial binning for quantification, we showed that dominant TCR clones were more abundant within the tumor cell compartment in all three analyzed patient samples (figure 5C), indicating that expanded TCR clones are more frequently in direct contact with cancer cells. These expanded T-cell clones were more often of the CD8 subtype, confirming the CD8 expansion observed in the bulk RNA-seq data (online supplemental figure S5 A and B). Taken together, the in situ location of TCR clones indicated an extension of CD8 effector cells that approximates cancer cells, suggesting a specific reaction.

DISCUSSION

Our study uncovers a significant variability of T-cell clonal expansion in human lung cancer tissue. The expansion, quantified as the Gini index, is associated with a specific molecular background (eg, EGFR, TP53), higher mutational load, and activated but also exhausted immune cell profiles. The clinical relevance of the findings is demonstrated, as patients with elevated TCR clonality benefit from checkpoint inhibitor therapies. Functional implications of these dominant clones are indicated by their in situ recovery as CD8 effector cells in proximity to cancer cells.

Our study is developed on the basis of previous developments of the bioinformatic pipelines, allowing for the precise alignment of TCR sequences from crude RNA-seq data to estimate the number of T-cell clones. ^{29 34} Our MiXCR approach was adopted from the study of Valpione *et al.* ³⁴ who analyzed TCR clonality in melanoma and lymphoma, respectively.

To describe the clonal distribution, we used the Gini index instead of entropy to describe the distribution of TCR clones, which emphasize unevenness and might be more sensitive to identifying clonal expansion.²⁰

There are few previous studies analyzing TCR clonality in diagnostic lung cancer samples. The study of Zhang et al⁴⁷ evaluated the tumor tissue of 10 patients who received neoadjuvant immunotherapy. They found that the entropy of TCR clones in the remaining tumor bed after immunotherapy correlated with the residual tumor cell viability and major pathological response. They also showed, using pretreatment and post-treatment blood samples, an expansion of corresponding dominant clones. In a comparable approach using a targeted RNA assay, Casarrubios and coworkers⁴⁸ confirmed those results in post-treatment tumor tissue. In addition, they found in the pretreatment tissue that the clonal space occupied by the top 1% pretreatment clones was associated with response to neoadjuvant therapy.

A more recent study from the group of Amos³² compared complex immune profiles in tumor and normal lung tissue from surgical specimens of 67 patients with NSCLC. Notably, their TCR clonality analysis identified substantially fewer T-cell clones (total number of reads) than in our study, although they used the same MiXCR as an alignment tool in their pipeline. This discrepancy might be due to a different quality of RNA-seq source data. However, analogous to our study, they found a higher TCR clonality in the adjacent normal tissue. A larger study analyzed TCR clonality in blood and tissue samples (tumor and adjacent normal lung) of 214 patients with a targeted RNA assay. Their findings indicated a strong relation between TCR entropy and specific immune cell profiles. When filtrating tumor TCR against blood clonality, they demonstrated that higher "tumor enriched" clonal expansion in the normal lung was associated with longer survival in the patient group after surgical resection.²⁵ The most recent study analyzed TCR clonality peripheral in blood lymphocytes before immunotherapy and linked higher clonal TCR richness to better response and higher risk of immune-related adverse events in a large NSCLC cohort. 49

Our study confirmed and extended previous findings in an independent, molecularly and clinically extensively annotated data set of patients with NSCLC. For the first time, we demonstrate that TCR clonality in pretreatment tissue samples is associated with the survival of patients with checkpoint inhibitor-treated NSCLC, while in operated patients, TCR clonality is not prognostic.

Our comparative analysis provided evidence that the clonal expansion of T cells is paralleled by the infiltration

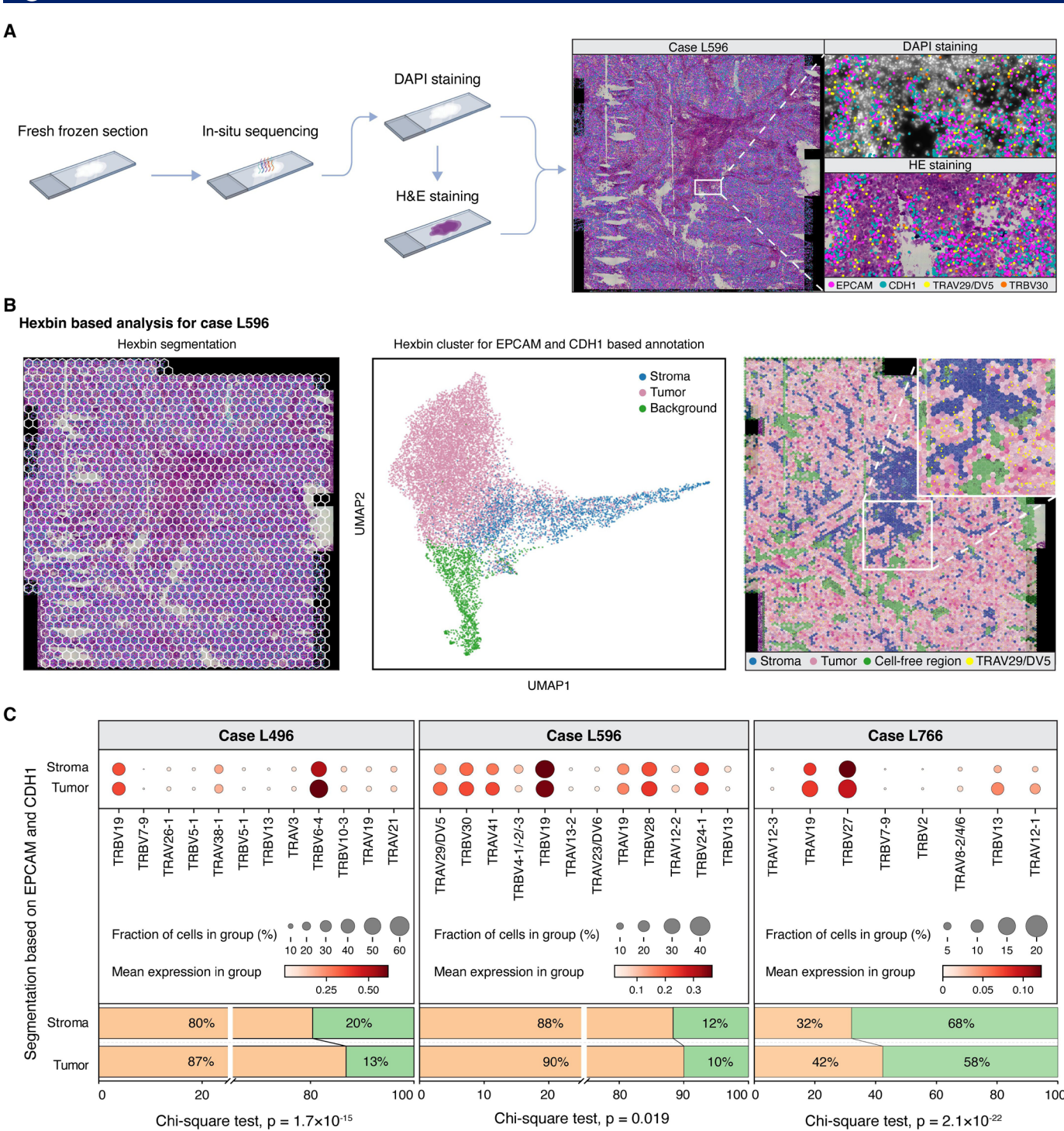


Figure 5 Hexbin-based analysis of in situ sequencing data. (A) In situ sequencing (ISS) workflow, illustrated by case L596. The right panel shows a stained image with markers for EPCAM, CDH1, as well as the TCR genes TRAV29/DV5 and TRBV30. (B) Hexbin-based analysis pipeline applied to the ISS data illustrated by case L596. The left image depicts the hexagonal segmentation of the ISS results, where each hexbin aggregates detected signals based on their spatial coordinates. The middle UMAP plot visualizes the clustering of all marker genes, with the tissue compartments (tumor vs stroma) annotated based on the expression levels of EPCAM and CDH1. UMAP clusters were used to compartmentalize the tissue section (right figure) into tumor, stroma, and background, along with the location of a dominant clone. (C) Comparison of dominant TCR clones between tumor and stroma compartments across three cases (L496, L596, L766). The dot plot illustrates the proportion of hexbins containing each dominant clone in tumor and stroma: the dot size indicates the fraction of hexbin containing the dominant clone. The color intensity indicates the mean expression of the dominant clone transcripts. X² tests were conducted to assess the distribution of dominant clones between tumor and stroma, with p-values indicated for each case. DAPI, 4',6-diamidino-2-phenylindole; TCR, T-cell receptor.

Hexbin without dominant clones

Hexbin with dominant clones

of CD8 effector cells in the tumor cell compartments, that are in direct contact with tumor cells. We confirmed this relation in the spatial multiplex IF analyses and even visualized these expanded T-cell clones in the in situ cancer environment by in situ RNA-seq. This in situ data positioned the expanded TCR clones closer to the tumor cells and confirmed that they are rather of CD8 subtype.

Together, the in situ findings strongly indicate that some expanded TCR clones are functionally related to tumor antigens. Therefore, it was not surprising that the potentially specific immune response coincided with an increase in inhibitory cell populations (CD163 M2-like macrophages) and markers of immune cell exhaustion (LAG3, PD-L1, PD-1), possibly counteracting any beneficial cytolytic response.

The observation that T-cell expansion was associated with an ineffective immune reaction might explain why higher TCR clonality in tumor tissue does not translate into a survival benefit in our surgically treated patient cohort and possibly also in the surgically treated cohort previously described by Reuben *et al*,²⁵ but is prognostic and predictive when checkpoint inhibitor therapy is applied. Therefore, our findings support the concept that the clonal expansion is tumor-antigen specific but ineffective and can thus potentially be therapeutically unleashed.

Still, a possible alternative explanation is that the TCR clonality serves as a strong surrogate for the "hot" immune environment and, therefore, is not directly related to a specific therapeutic antitumor immune reaction. Although our Uppsala cohort presents an extensive and highly detailed TCR clonality data set, the immunotherapy cohort consisted of only nine patients. The low number reflects the problem that fresh tissue is usually not available from patients with advanced cancer but is still required to obtain high-quality RNA for the TCR clonality analysis. This limitation hinders further evaluation of the TCR clonality, based on broad RNA-seq, as a predictive biomarker for immune therapy. As an alternative, a more robust, targeted DNA-based assay could be better suited for analyzing minute FFPE material in clinical diagnostics. Current targeted approaches, using multiplex PCR libraries or 5' RACE libraries for the TCR CDR3 repertoire sequencing, also have the advantage of yielding exceedingly higher unique TCR clone numbers (>10,000 per sample)⁵⁰ than our MiXCR bulk RNA-seq method (range: 36-911 unique TCR clones). However, neither transcriptomic nor targeted sequencing on bulk RNA/ DNA provides $\alpha\beta$ -chain pairing information, which limits true clonotyping or functional antigen prediction. These obstacles are addressed by single-cell TCR sequencing, allowing even the integration of transcriptomic data on a cellular level.^{51 52} An alternative approach is targeted spatial transcriptomics, which includes a detailed characterization of the cellular ecosystems within tissues.^{53–55} However, as shown in our present study and supported by others, spatial transcriptomics remains limited in sensitivity-particularly for stromal cells-and thus cannot

reliably provide high-sensitivity $\alpha\beta$ -chain pairing information. ⁵⁶ Of note, both single-cell TCR sequencing and targeted spatial transcriptomics are expensive, not well-suited for high-throughput applications, and require the handling of fresh tissue, which limits their clinical applications.

With this background, we believe that our approach has its highest value in approximating clonal frequency distributions. It should be emphasized that the number and richness of detected TCR clones in our RNA-seq data were higher than in previous studies that used bulk RNA-seq data. Our results were further validated against an independent CE-marked, DNA-based assay (Lympho-Track), which is used in clinical diagnostics to identify and track clonality in lymphocytic diseases. The strong congruence confirmed the robustness of our pipeline and the accuracy of the TCR data set we used for comparative analysis.

In conclusion, our study linked T-cell clonal expansion to relevant molecular and immunophenotypes of NSCLC, localized the TCR clones in patient tissue, and provided evidence that the analysis has potential as a predictive marker delineating a group of patients that will benefit from checkpoint inhibition. Our publicly available, extensive data set also presents a unique source for more focused studies, aiming to understand the mechanism of immune cell activation in lung cancer. Hopefully, this will contribute to improving the current therapeutic options, which currently offer only a limited overall response.

Author affiliations

¹Department of Immunology, Genetics and Pathology, Uppsala University, Uppsala, Uppsala County, Sweden

²Science for Life Laboratory, Department of Biochemistry and Biophysics, Stockholm University, Stockholm, Stockholm County, Sweden

³Division of Molecular and Genomic Pathology, Department of Pathology, Kobe University Graduate School of Medicine, Kobe, Japan

⁴Molecular Oncology Group, Vall d'Hebron Institute of Oncology, Barcelona, Spain ⁵Dept. of Proteomics and Signal Transduction, Max Planck Institute of Biochemistry, Martinsried, Germany

⁶Division of Pathology, Lund University, Lund, Sweden

⁷Department of Microbiology, Tumor and Cell Biology, Karolinska Institutet, Stockholm, Stockholm County, Sweden

⁸Department of Translational Medicine, Lund University, Lund, Sweden ⁹Center for Cancer Biomarkers, Department of Clinical Medicine, University of Bergen, Bergen, Norway

Contributors HY contributed to conceptualization, methodology, software, formal analysis, investigation, resources, data curation and writing, reviewing and editing the article. AMag contributed to methodology, formal analysis, investigation and reviewing and editing the article. MPC, R-mA and MH contributed to methodology and reviewing and editing the article. AL, AMez, MB, MMZ and JSMM contributed to formal analysis, data curation, resources, reviewing and editing the article. AMet contributed to methodology. HB, JB, KK and KL contributed to resources, reviewing and editing the article. MN contributed to conceptualization, methodology, software, validation, data curation and writing, reviewing and editing the article. CS contributed to conceptualization, methodology, validation, formal analysis, supervision, project administration, funding acquisition, writing, reviewing and editing the article. PM contributed to conceptualization, methodology, validation, resources, supervision, project administration, funding acquisition, writing, reviewing and editing the article. PM is the guarantor of this study. During the preparation of this work, the authors used ChatGPT 4.0 (Open Al) for language editing. After using this tool, the authors reviewed and edited the content as needed and take full responsibility for the content of the published article.



Funding This study was partly supported by the Sjöberg Foundation, Sweden; the Swedish Cancer Society, the Lions Cancer Foundation Uppsala, Sweden, and the Swedish Government Grant for Clinical Research. CS holds a starting grant from the Trond Mohn Foundation. We thank the Research and Development Unit of the Pathology Department of the University Hospital Uppsala for their continuous support as well as the Uppsala Biobank. The funders did not directly participate in conducting this research.

Competing interests No, there are no competing interests.

Patient consent for publication Not applicable.

Ethics approval This study involves human participants and was approved by Ethical Review Board in Uppsala, #2012/532. The study is a retrospective analysis using archived samples from patients with lung cancer who underwent surgery between 2006 and 2010 at the Uppsala University Hospital. Most patients were already dead when the study was initiated; therefore, the study was approved without patient consent.

Provenance and peer review Not commissioned; externally peer reviewed.

Data availability statement Data are available in a public, open access repository.

Supplemental material This content has been supplied by the author(s). It has not been vetted by BMJ Publishing Group Limited (BMJ) and may not have been peer-reviewed. Any opinions or recommendations discussed are solely those of the author(s) and are not endorsed by BMJ. BMJ disclaims all liability and responsibility arising from any reliance placed on the content. Where the content includes any translated material, BMJ does not warrant the accuracy and reliability of the translations (including but not limited to local regulations, clinical guidelines, terminology, drug names and drug dosages), and is not responsible for any error and/or omissions arising from translation and adaptation or otherwise.

Open access This is an open access article distributed in accordance with the Creative Commons Attribution Non Commercial (CC BY-NC 4.0) license, which permits others to distribute, remix, adapt, build upon this work non-commercially, and license their derivative works on different terms, provided the original work is properly cited, appropriate credit is given, any changes made indicated, and the use is non-commercial. See http://creativecommons.org/licenses/by-nc/4.0/.

ORCID iDs

Hui Yu http://orcid.org/0009-0000-0563-3243 Patrick Micke http://orcid.org/0000-0003-1210-5961

REFERENCES

- 1 Topalian SL, Pardoll DM. Neoadjuvant anti-PD-1-based immunotherapy: evolving a new standard of care. *J Immunother Cancer* 2025;13:e010833.
- 2 Cortellini A, Brunetti L, Di Fazio GR, et al. Determinants of 5-year survival in patients with advanced NSCLC with PD-L1≥50% treated with first-line pembrolizumab outside of clinical trials: results from the Pembro-real 5Y global registry. J Immunother Cancer 2025:13:e010674.
- 3 Fridman WH, Pagès F, Sautès-Fridman C, et al. The immune contexture in human tumours: impact on clinical outcome. Nat Rev Cancer 2012;12:298–306.
- 4 Edlund K, Madjar K, Mattsson JSM, et al. Prognostic Impact of Tumor Cell Programmed Death Ligand 1 Expression and Immune Cell Infiltration in NSCLC. J Thorac Oncol 2019;14:628–40.
- 5 Henick BS, Villarroel-Espindola F, Datar I, et al. Quantitative tissue analysis and role of myeloid cells in non-small cell lung cancer. J Immunother Cancer 2022;10:e005025.
- 6 Backman M, Strell C, Lindberg A, et al. n.d. Spatial Immunophenotyping of the Tumor Microenvironment in Non-Small Cell Lung Cancer. SSRN Journal.
- 7 Lopez de Rodas M, Villalba-Esparza M, Sanmamed MF, et al. Biological and clinical significance of tumour-infiltrating lymphocytes in the era of immunotherapy: a multidimensional approach. Nat Rev Clin Oncol 2025;22:163–81.
- 8 Paijens ST, Vledder A, de Bruyn M, et al. Tumor-infiltrating lymphocytes in the immunotherapy era. Cell Mol Immunol 2021:18:842–59.
- 9 Miller BC, Sen DR, Al Abosy R, et al. Subsets of exhausted CD8⁺ T cells differentially mediate tumor control and respond to checkpoint blockade. Nat Immunol 2019;20:326–36.
- 10 Parra ER, Villalobos P, Zhang J, et al. Immunohistochemical and Image Analysis-Based Study Shows That Several Immune

- Checkpoints are Co-expressed in Non-Small Cell Lung Carcinoma Tumors. *J Thorac Oncol* 2018;13:779.
- 11 Schiza A, Thurfjell V, Stenmark Tullberg A, et al. Tumour-infiltrating lymphocytes add prognostic information for patients with low-risk DCIS: findings from the SweDCIS randomised radiotherapy trial. Eur J Cancer 2022;168:128–37.
- 12 Backman M, La Fleur L, Kurppa P, et al. Infiltration of NK and plasma cells is associated with a distinct immune subset in non-small cell lung cancer. J Pathol 2021;255:243–56.
- 13 Elfving H, Thurfjell V, Mattsson JSM, et al. Tumor Heterogeneity Confounds Lymphocyte Metrics in Diagnostic Lung Cancer Biopsies. Arch Pathol Lab Med 2024;148:e18–24.
- 14 Shirasawa M, Yoshida T, Shimoda Y, et al. Differential Immune-Related Microenvironment Determines Programmed Cell Death Protein-1/Programmed Death-Ligand 1 Blockade Efficacy in Patients With Advanced NSCLC. J Thorac Oncol 2021;16:2078–90.
- 15 Gros A, Robbins PF, Yao X, et al. tumor-reactive repertoire infiltrating human tumors. J Clin Invest 2014;124:73639:2246–59:.
- 16 Pasetto A, Gros A, Robbins PF, et al. Tumor- and Neoantigen-Reactive T-cell Receptors Can Be Identified Based on Their Frequency in Fresh Tumor. Cancer Immunol Res 2016;4:734–43.
- 17 Chapman NM, Chi H. Hallmarks of T-cell Exit from Quiescence. Cancer Immunol Res 2018;6:502–8.
- 18 Chapman NM, Boothby MR, Chi H. Metabolic coordination of T cell quiescence and activation. Nat Rev Immunol 2020;20:55–70.
- 19 Kaech SM, Wherry EJ, Ahmed R. Effector and memory T-cell differentiation: implications for vaccine development. *Nat Rev Immunol* 2002;2:251–62.
- 20 Chiffelle J, Genolet R, Perez MA, et al. T-cell repertoire analysis and metrics of diversity and clonality. Curr Opin Biotechnol 2020;65:284–95.
- 21 Afzal S, Gil-Farina I, Gabriel R, et al. Systematic comparative study of computational methods for T-cell receptor sequencing data analysis. Brief Bioinform 2019;20:222–34.
- 22 Wang H-W, Raffeld M. Molecular assessment of clonality in lymphoid neoplasms. *Semin Hematol* 2019;56:37–45.
- 23 Paulsen K, Marincevic M, Cavelier L, et al. LymphoTrack Is Equally Sensitive as PCR GeneScan and Sanger Sequencing for Detection of Clonal Rearrangements in ALL Patients. *Diagnostics (Basel)* 2022:12:1389.
- 24 Aoki H, Shichino S, Matsushima K, et al. Revealing Clonal Responses of Tumor-Reactive T-Cells Through T Cell Receptor Repertoire Analysis. *Front Immunol* 2022;13:807696.
- 25 Reuben A, Zhang J, Chiou S-H, et al. Comprehensive T cell repertoire characterization of non-small cell lung cancer. Nat Commun 2020;11:603.
- 26 McNeel DG. TCR diversity a universal cancer immunotherapy biomarker? J Immunother Cancer 2016;4:69.
- 27 Tumeh PC, Harview CL, Yearley JH, et al. PD-1 blockade induces responses by inhibiting adaptive immune resistance. Nature New Biol 2014;515:568–71.
- Yusko E, Vignali M, Wilson RK, et al. Association of Tumor Microenvironment T-cell Repertoire and Mutational Load with Clinical Outcome after Sequential Checkpoint Blockade in Melanoma. Cancer Immunol Res 2019;7:458–65.
- 29 Valpione S, Mundra PA, Galvani E, et al. The T cell receptor repertoire of tumor infiltrating T cells is predictive and prognostic for cancer survival. Nat Commun 2021;12:4098.
- 30 Bolotin DA, Poslavsky S, Mitrophanov I, et al. MiXCR: software for comprehensive adaptive immunity profiling. Nat Methods 2015;12:380–1
- 31 Rosati E, Dowds CM, Liaskou E, et al. Overview of methodologies for T-cell receptor repertoire analysis. BMC Biotechnol 2017;17:61.
- 32 Cheng C, Nguyen TT, Tang M, et al. Immune Infiltration in Tumor and Adjacent Non-Neoplastic Regions Codetermines Patient Clinical Outcomes in Early-Stage Lung Cancer. J Thorac Oncol 2023;18:1184–98.
- 33 Naulaerts S, Datsi A, Borras DM, et al. Multiomics and spatial mapping characterizes human CD8⁺ T cell states in cancer. Sci Transl Med 2023;15:eadd1016.
- 34 Farmanbar A, Kneller R, Firouzi S. RNA sequencing identifies clonal structure of T-cell repertoires in patients with adult T-cell leukemia/ lymphoma. npi Genom Med 2019:4:10.
- 35 Djureinovic D, Hallström BM, Horie M, et al. Profiling cancer testis antigens in non-small-cell lung cancer. JCl Insight 2016;1:e86837.
- 36 Cho J-W, Hong MH, Ha S-J, et al. Genome-wide identification of differentially methylated promoters and enhancers associated with response to anti-PD-1 therapy in non-small cell lung cancer. Exp Mol Med 2020;52:1550–63.
- 37 Mezheyeuski A, Bergsland CH, Backman M, et al. Multispectral imaging for quantitative and compartment-specific immune infiltrates



- reveals distinct immune profiles that classify lung cancer patients. *J Pathol* 2018;244:421–31.
- 38 Mezheyeuski A, Backman M, Mattsson J, et al. An immune score reflecting pro- and anti-tumoural balance of tumour microenvironment has major prognostic impact and predicts immunotherapy response in solid cancers. *EBioMedicine* 2023;88:104452.
- 39 La Fleur L, Falk-Sörqvist E, Smeds P, et al. Mutation patterns in a population-based non-small cell lung cancer cohort and prognostic impact of concomitant mutations in KRAS and TP53 or STK11. Lung Cancer (Auckl) 2019;130:50–8.
- 40 Lee H, Langseth CM, Salas SM, et al. Open-source, high-throughput targeted in situ transcriptomics for developmental and tissue biology. Development 2024;151:dev202448.
- 41 Lee H, Marco Salas S, Gyllborg D, et al. Direct RNA targeted in situ sequencing for transcriptomic profiling in tissue. Sci Rep 2022:12:7976
- 42 Mika J, Polanska A, Blenman KR, et al. A comprehensive evaluation of diversity measures for TCR repertoire profiling. BMC Biol 2025:23:133.
- 43 McLane LM, Abdel-Hakeem MS, Wherry EJ. CD8 T Cell Exhaustion During Chronic Viral Infection and Cancer. *Annu Rev Immunol* 2019;37:457–95.
- 44 Blank CU, Haining WN, Held W, et al. Defining "T cell exhaustion".

 Nat Rev Immunol 2019:19:665–74.
- 45 Kim CG, Kim G, Kim KH, et al. Distinct exhaustion features of T lymphocytes shape the tumor-immune microenvironment with therapeutic implication in patients with non-small-cell lung cancer. J Immunother Cancer 2021;9:e002780.
- 46 Lopez de Rodas M, Schalper KA. Tumour antigen-induced T cell exhaustion - the archenemy of immune-hot malignancies. Nat Rev Clin Oncol 2021;18:749–50.
- 47 Zhang J, Ji Z, Caushi JX, et al. Compartmental Analysis of Tcell Clonal Dynamics as a Function of Pathologic Response to

- Neoadjuvant PD-1 Blockade in Resectable Non–Small Cell Lung Cancer. *Clin Cancer Res* 2020;26:1327–37.
- 48 Casarrubios M, Cruz-Bermúdez A, Nadal E, et al. Pretreatment Tissue TCR Repertoire Evenness Is Associated with Complete Pathologic Response in Patients with NSCLC Receiving Neoadjuvant Chemoimmunotherapy. Clin Cancer Res 2021;27:5878–90.
- 49 Altan M, Li R, Li Z, et al. High peripheral T cell diversity is associated with lower risk of toxicity and superior response to dual immune checkpoint inhibitor therapy in patients with metastatic NSCLC. J Immunother Cancer 2024;12:e008950.
- 50 Frank ML, Lu K, Erdogan C, et al. T-Cell Receptor Repertoire Sequencing in the Era of Cancer Immunotherapy. Clin Cancer Res 2023;29:994–1008.
- 51 Pai JA, Satpathy AT. High-throughput and single-cell T cell receptor sequencing technologies. *Nat Methods* 2021;18:881–92.
- 52 Gao S, Wu Z, Arnold B, et al. Single-cell RNA sequencing coupled to TCR profiling of large granular lymphocyte leukemia T cells. Nat Commun 2022;13:1982.
- 53 Svedlund J, Strell C, Qian X, et al. Generation of in situ sequencing based OncoMaps to spatially resolve gene expression profiles of diagnostic and prognostic markers in breast cancer. EBioMedicine 2019;48:212–23.
- 54 Andersson A, Larsson L, Stenbeck L, et al. Spatial deconvolution of HER2-positive breast cancer delineates tumor-associated cell type interactions. Nat Commun 2021;12:6012.
- 55 Lomakin A, Svedlund J, Strell C, et al. Spatial genomics maps the structure, nature and evolution of cancer clones. Nature New Biol 2022;611:594–602.
- 56 Engblom C, Thrane K, Lin Q, et al. Spatial transcriptomics of B cell and T cell receptors reveals lymphocyte clonal dynamics. Science 2023;382:eadf8486.